



## Great Plains Precipitation and Its SST Links in Twentieth-Century Climate Simulations, and Twenty-First- and Twenty-Second-Century Climate Projections

ALFREDO RUIZ-BARRADAS

*Department of Atmospheric and Oceanic Science, University of Maryland, College Park, College Park, Maryland*

SUMANT NIGAM

*Department of Atmospheric and Oceanic Science, and Earth System Science Interdisciplinary Center, University of Maryland, College Park, College Park, Maryland*

(Manuscript received 1 April 2009, in final form 19 May 2010)

### ABSTRACT

The present work assesses spring and summer precipitation over North America as well as summer precipitation variability over the central United States and its SST links in simulations of the twentieth-century climate and projections of the twenty-first- and twenty-second-century climates for the A1B scenario.

The observed spatial structure of spring and summer precipitation poses a challenge for models, particularly over the western and central United States. Tendencies in spring precipitation in the twenty-first century agree with the observed ones at the end of the twentieth century over a wetter north-central and a drier southwestern United States, and a drier southeastern Mexico. Projected wetter springs over the Great Plains in the twenty-first and twenty-second centuries are associated with an increase in the number of extreme springs. In contrast, projected summer tendencies have demonstrated little consistency. The associated observed changes in SSTs bear the global warming footprint, which is not well captured in the twentieth-century climate simulations.

Precipitation variability over the Great Plains presents a coherent picture in spring but not in summer. Models project an increase in springtime precipitation variability owing to an increased number of extreme springs. The number of extreme droughty (pluvial) events during the spring–fall part of the year is under(over)estimated in the twentieth century without consistent projections.

Summer precipitation variability over the Great Plains is linked to SSTs over the Pacific and Atlantic Oceans, with no apparent ENSO link in spite of the exaggerated variability in the equatorial Pacific in climate simulations; this has been identified already in observations and atmospheric models forced with historical SSTs. This link is concealed due to the increased warming in the twenty-first century. Deficiencies in land surface–atmosphere interactions and global teleconnections in the climate models prevent them from a better portrayal of summer precipitation variability in the central United States.

### 1. Introduction

Global climate change due to increased man-induced greenhouse gases threatens societies and ecosystems around the planet. In the same way that climate is not equal everywhere, climate change will have different impacts around the globe. Thus, interest in regional climate change, especially hydroclimate, has increased. As a result of society's dependence on water supply, as well

as the need for prevention and mitigation of extreme hydroclimate events, current and projected regional hydroclimate research has become an issue of fundamental interest.

Carbon dioxide is the most important greenhouse gas that fuels the discussion of anthropogenic climate change. Increased burning of fossil fuels and deforestation have caused carbon dioxide concentrations to increase globally in the twentieth century. In an effort to simulate past, present, and future climates under the stress of growing greenhouse concentrations, the World Meteorological Organization through the Intergovernmental Panel on Climate Change (IPCC), has led the assessment of climate simulations of the twentieth century and climate

---

*Corresponding author address:* Alfredo Ruiz-Barradas, 3405 Computer and Space Sciences Bldg., University of Maryland, College Park, College Park, MD 20742-2425.  
E-mail: alfredo@atmos.umd.edu

projections of the twenty-first and twenty-second centuries from models participating in the World Climate Research Programme (WCRP) Coupled Model Inter-comparison Project phase 3 (CMIP3). Findings of the latest assessment are included in the Fourth Assessment Report, highlighting the anthropogenic nature of the current global warming trend (Solomon et al. 2007).

Some of the most difficult aspects of understanding and projecting changes in regional hydroclimate are associated with changes in the circulation of the atmosphere and oceans. This is particularly challenging over the central United States where regional hydroclimate strongly depends on the moisture transport from the Gulf of Mexico via the Great Plains low-level jet (e.g., Ruiz-Barradas and Nigam 2005, 2006; Cook et al. 2008; Weaver and Nigam 2008). Several empirical and atmosphere-model-based studies have documented the importance of SST links of the central U.S. hydroclimate. Both Pacific SST variability (e.g., Ting and Wang 1997; Barlow et al. 2001; Schubert et al. 2004; Seager et al. 2005; Ruiz-Barradas and Nigam 2005, 2010; McCabe et al. 2004, 2008) and Atlantic SST variability (e.g., Enfield et al. 2001; Ruiz-Barradas and Nigam 2005, 2010; Sutton and Hodson 2005; Wang et al. 2006; McCabe et al. 2004, 2008) have the potential to induce anomalous hydroclimatic conditions over North America. It has been shown that SST structures with contrasting signs in the Pacific and Atlantic Oceans [cold (warm) Pacific and a warm (cold) Atlantic] are conducive to the most extreme [droughty (pluvial)] conditions over the central Great Plains (e.g., Hoerling and Kumar 2003; Schubert et al. 2009). If both basins have the same sign, they are still capable of producing extreme hydroclimatic conditions over the central United States (Schubert et al. 2009). In any case, model experiments suggest that the tropical component largely forces the central U.S. hydroclimate variability (e.g., Schubert et al. 2004, 2009; Seager et al. 2005; Sutton and Hodson 2005); however, the nature of the tropical anomalies needs some clarification as they may be the result of extratropical activities.

The influence of the oceans in generating precipitation variability in several models is obscured by their overactive local land surface–atmosphere interactions (Ruiz-Barradas and Nigam 2005, 2006). Simulations of the twentieth-century climate based on some models from international research centers, which are part of the CMIP3 multimodel dataset (Meehl et al. 2007), revealed difficulties in two aspects of their simulations: the observed distribution of climatological summer precipitation and the observed link between precipitation variability and moisture flux convergence over the central United States (Ruiz-Barradas and Nigam 2006). While it is likely

that at the end of the twenty-first century the northern half of the United States (north of  $\sim 45^\circ\text{N}$ ) will experience an increase in winter precipitation, the western United States will suffer a deficit in summer precipitation, leaving the conditions of the central United States unclear during spring and summer seasons (e.g., chapter 11 in Solomon et al. 2007). In a recent study by Cook et al. (2008), climate projections of the twenty-first century were analyzed from models of the CMIP3 dataset under a scenario of rapid  $\text{CO}_2$  increase [Special Report on Emissions Scenarios (SRES) A2, see Nakicenovic et al. (2000)]; the study concluded that over the central United States at the end of the twenty-first century, climatological springtime precipitation will increase as a result of an increase in the intensity of the Great Plains low-level jet.

The present paper assesses North American climatological spring and summer precipitation, as well as warm-season precipitation variability over the Great Plains and its links with SSTs from simulations of the twentieth-century climate (20C3M) and from climate projections of the twenty-first and twenty-second centuries. The models used are from leading international climate research institutions that contributed to the WCRP CMIP3 multimodel dataset. The purpose of this study is to find common traits between observations, simulations, and projections of climatological precipitation over North America, as well as to provide insights into the current and projected SST structures that may be driving hydroclimate variability over the central United States in the present and future centuries. The paper is organized beginning with section 2, which provides some basic information about the models and runs, in addition to the observational datasets used as reference for the twentieth-century climate simulations. Next, section 3 analyzes spring and summer climatology over North America and its changes. Section 4 elaborates on precipitation variability, including the presence of extreme events over the Great Plains; section 5 contrasts the summer SST structures associated with their change and variability in the twentieth century; and section 6 analyses the global SST links of Great Plains summer precipitation variability. Finally, the paper ends with section 7, which summarizes the main conclusions.

## 2. Datasets and methods

Simulations and projections from four models are assessed from representatives of major climate research centers in the world, including 1) the National Center for Atmospheric Research Community Climate System Model, version 3 (CCSM3) [Collins et al. (2006) and additional references in the CCSM special issue in the *Journal of Climate*, 2006, Vol. 19, No. 11], 2) the NOAA/Geophysical Fluid Dynamics Laboratory (GFDL) Climate

TABLE 1. Basic details of the models analyzed: name, horizontal and vertical resolution of the atmospheric model, years of integration for the historical twentieth-century climate simulation (20C3M), and the projected climate for the twenty-first and twenty-second centuries (A1B), and the ensemble member used in the analysis.

Model	Resolution (atmosphere)	Years (20C3M/A1B)	Ensemble
CCSM3	T85, L26	1870–1999/2000–2349	7
GFDL CM2.1	M45, L24	1861–2000/2001–2300	1
HadCM3	3.75° lon × 2.5° lat, L19	1860–1999/2000–2199	1
ECHAM5/MPI-OM	T63, L32	1860–2000/2001–2300	2

Model version 2.1 (CM2.1) (Delworth et al. 2006), 3) the third climate configuration of the Met Office Unified Model (HadCM3) (Gordon et al. 2000; Pope et al. 2000), and 4) the European Centre Hamburg Model (ECHAM5)/Max Planck Institute Ocean Model (MPI-OM) (Roeckner et al. 2003; Marsland et al. 2003). Apart from ECHAM5/MPI-OM climate model, the others were assessed in their capacity to simulate the observed interannual variability of Great Plains precipitation and its links to moisture fluxes in the twentieth century in a previous study (Ruiz-Barradas and Nigam 2006). From this analysis it was found that while the HadCM3 best portrays the observed relationship between precipitation variability and moisture flux convergence, CCSM3 and GFDL CM2.1 both prioritize a precipitation–evaporation relationship; additional analyzes (not shown) on ECHAM5/MPI-OM indicate that this model behaves like the HadCM3 regarding the summer precipitation variability over the central Great Plains. Details of the models and runs analyzed in the current study are summarized in Table 1.

Historical simulations of the twentieth century are initialized from a point early in the preindustrial period. These simulations come from coupled GCMs that are being forced by observed solar irradiance, volcanic and anthropogenic aerosols, and atmospheric concentrations of ozone, carbon dioxide, and other well-mixed greenhouse gases (Solomon 2007, see chapter 2). In general, the model simulations extend over a century, starting in the second half of the 1800s and ending in 1999 for some and 2000 for others (Table 1).

The climate projections of the twenty-first and twenty-second centuries that are analyzed are runs under the A1B emission scenario, that is, SRES A1B, (Nakicenovic et al. 2000). The A1B scenario describes a world in the future with very rapid economic growth in the twenty-first century, characterized by the rapid introduction of new and more efficient technologies, and where global population peaks in midcentury and declines thereafter. Under this scenario, fossil fuels and other energy sources are balanced in the sense that there is not a heavy dependence on one particular source of energy over another. Initial conditions in the SRES A1B runs are from

simulations of the climate at the end of the twentieth century. Carbon dioxide mixing ratios in these runs change from 369 ppmv in the year 2000 to 717 ppmv in 2100; the CO<sub>2</sub> concentration almost doubles at the end of the twenty-first-century simulations after which it is fixed during the twenty-second century.

Observed precipitation for the twentieth century is obtained from the U.K. Climate Research Unit high-resolution gridded dataset, version 2.1 (CRUTS2.1; Mitchell 2005). This dataset includes monthly temperature and precipitation data on a 0.5° grid for land areas of the globe and spans the time period from 1901 through 2002. An observed global Palmer Drought Severity Index (PDSI) is also used (Dai et al. 2004); the dataset is defined over global land areas on a 2.5° grid at monthly resolution for the time period from 1870 to 2003 using in situ temperature and precipitation data. The SST links are then obtained using the Hadley Centre's Sea Ice and SST analysis that spans the time period from 1870 to 2002 on a 1° grid (Rayner et al. 2003), but is used on a coarser 5° × 2.5° grid.

Unless noted otherwise, climatology and long-term variability of the twentieth, twenty-first, and twenty-second centuries span the following 99-yr base periods: 1901–99, 2001–99, and 2101–99. To avoid intraseasonal variability, the basic data is seasonal and defined in terms of the typical 3-month means: December–February for winter, March–May for spring, June–August for summer, and September–November for fall; thus, for a given century the data starts in spring and ends in fall.

### 3. Precipitation climatology and change

Spring and summer seasons comprise the bulk of the distribution and amount of precipitation over North America, particularly in the central United States (east of the 100°W meridian) and Mexico; its amount and distribution can lead to conditions of normality, abundance, or scarcity for the region. The climatological march of the seasons brings routine or normal conditions to a region, so it must be one of the basic points of evaluation in any climate simulation. Climatological spring and summer precipitation in simulations of the twentieth

century and projections of the twenty-first and twenty-second centuries are analyzed here.

### a. Climatology

Spring and summer climatologies of precipitation in the simulations of the twentieth century are compared against observations and displayed in Fig. 1. Observations reveal a dry west and humid east over the United States in the spring and summer seasons. Also apparent are an increase in precipitation from spring to summer through the central United States and a decrease over the Pacific Northwest. Regions of maximum precipitation are seen through the southern Gulf States in spring and along the coastal regions of the gulf and south Atlantic states in summer. The dry spring and wet summer seasons in Mexico are also evident along the coasts, sierras, and central plateau.

Models reveal, with the exception of CCSM3, a wetter western United States in spring and wetter central United States in summer when compared against observations. Across all models, and following the general seasonal evolution seen in observations, precipitation increases over the central United States from spring to summer. Models reproduce the increase in precipitation over Mexico from spring to summer; however, they only do so on the western coast and fail to do so on the eastern side, most likely because the coarse resolution in the models prevent them from a proper representation of the eastern sierra as well as the tropical systems that interact with it (particularly in HadCM3). The oceanic part, however, suggests that the land–ocean competition for convection in the models is very large in summer and pushes the ITCZ very far to the north along the Mexican northwest. The maximum over the Pacific Northwest, seen in observations in spring, is reasonably reproduced by the models, in spite of their resolution, as well as its subsequent reduction in summer; this is likely to happen in the models owing to vorticity balance considerations associated with the Aleutian low and Pacific high seasonal appearance (Nigam and Ruiz-Barradas 2006). Observations also reveal that the maximum of spring precipitation over the United States emerges from the eastern Gulf of Mexico states; however, the models seem to reveal that the maximum of spring precipitation comes out of the east. On the other hand, the maximum of summer precipitation in observations lying along the coasts of the gulf and southern Atlantic states is reproduced with varied success by the models.

### b. Projected changes

Comparisons of the climate projections with the simulated climate of the twentieth century provide a

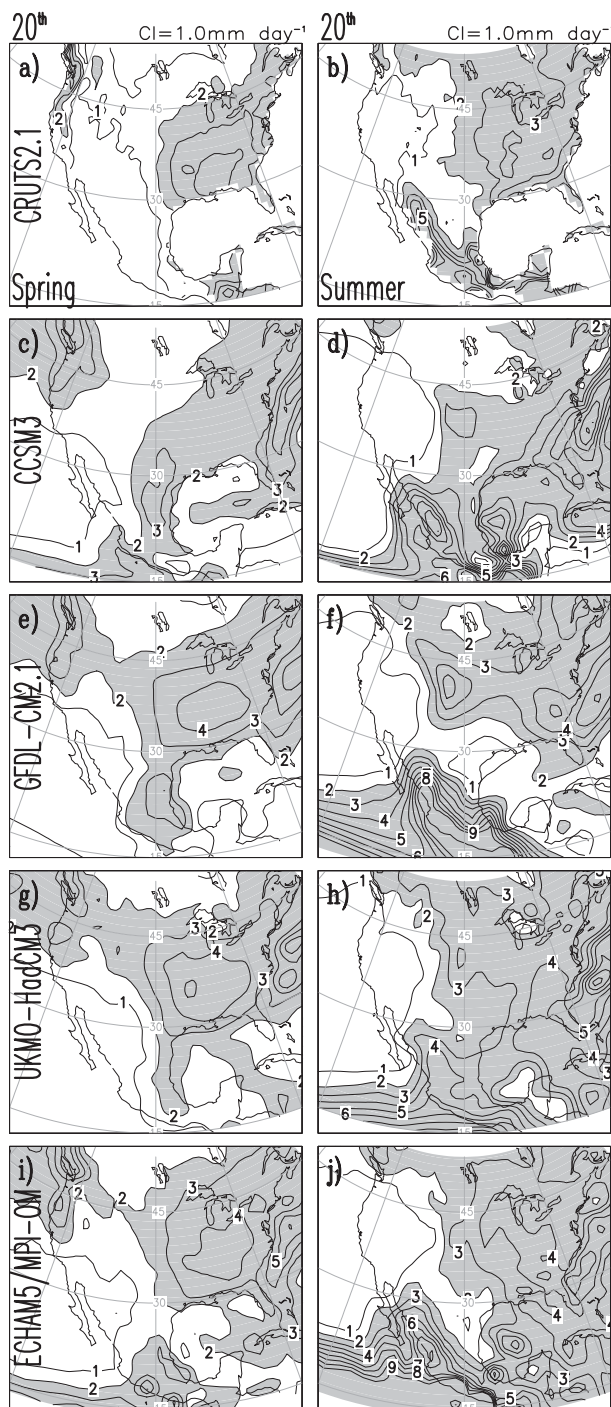


FIG. 1. (left) Spring (MAM) and (right) summer (JJA) precipitation climatology during the twentieth century (1901–99) in observations and coupled model simulations. (a),(b) CRUTS2.1, (c),(d) CCSM3, (e),(f) GFDL CM2.1, (g),(h) HadCM3, and (i),(j) ECHAM5/MPI-OM. Contour interval is  $1 \text{ mm day}^{-1}$  and shading is for values equal or larger than  $2 \text{ mm day}^{-1}$ .

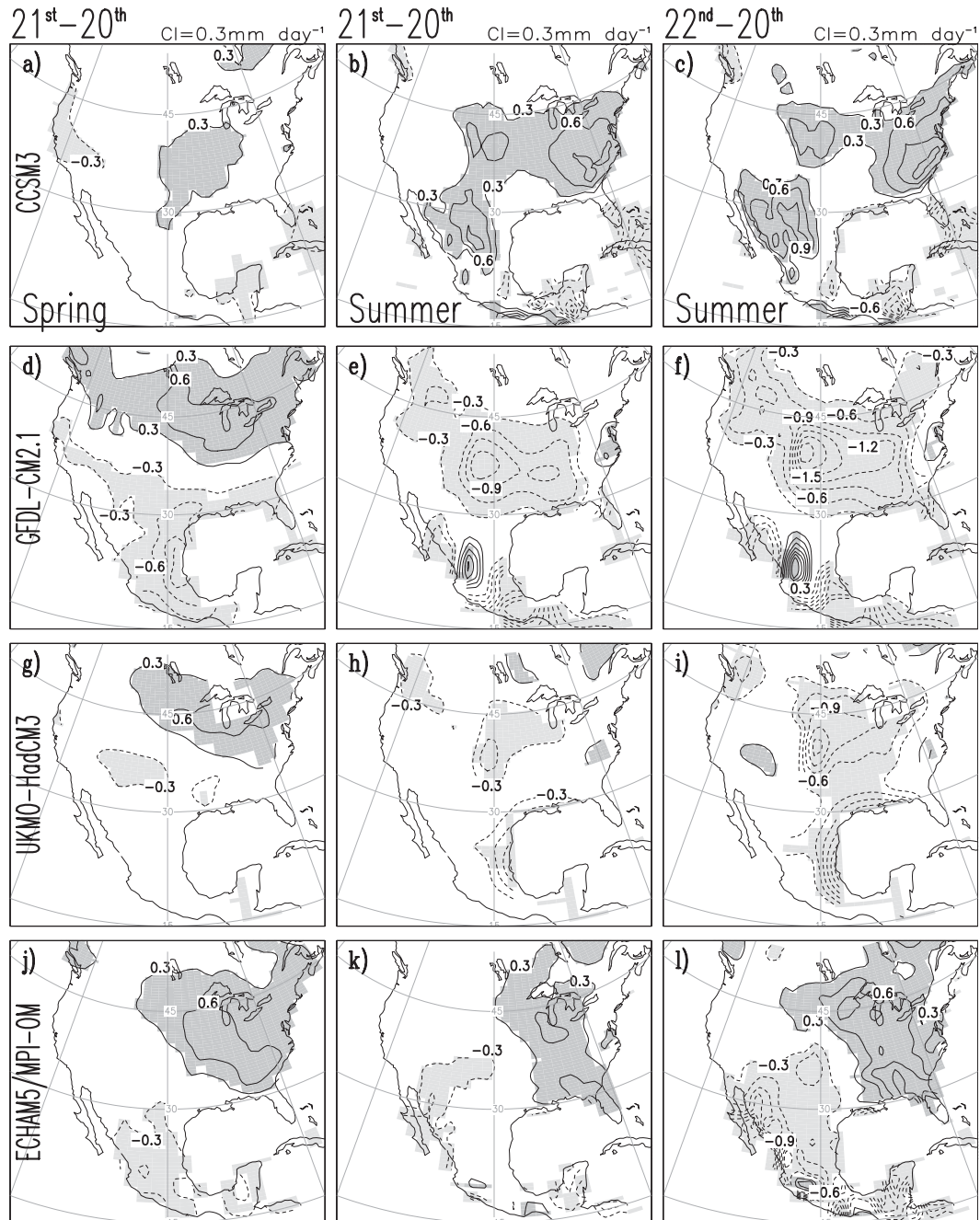


FIG. 2. Differences between the twenty-first-century projections (2001–99) and twentieth-century simulations (1901–99) of (left) spring and (middle) summer precipitation climatologies, and (right) between the twenty-second-century projections (2101–99) and the twentieth-century simulations of summer precipitation climatologies for (a)–(c) CCSM3, (d)–(f) GFDL CM2.1, (g)–(i) HadCM3, and (j)–(l) ECHAM5/MPI-OM. Contour interval is  $0.3 \text{ mm day}^{-1}$ , and dark (light) shading for positive (negative) differences larger than  $|\pm 0.3| \text{ mm day}^{-1}$ ; shaded differences are significant according to a one-tailed Student's  $t$  test at the 0.10 level.

reference to assess the climate projections under the scenario A1B in which carbon dioxide concentrations almost double in the twenty-first century and stabilize during the twenty-second century. Figure 2 displays

differences in spring and summer climatologies of the twenty-first century, as well as the summer climatology of the twenty-second century, with respect to the corresponding seasonal climatologies in the twentieth

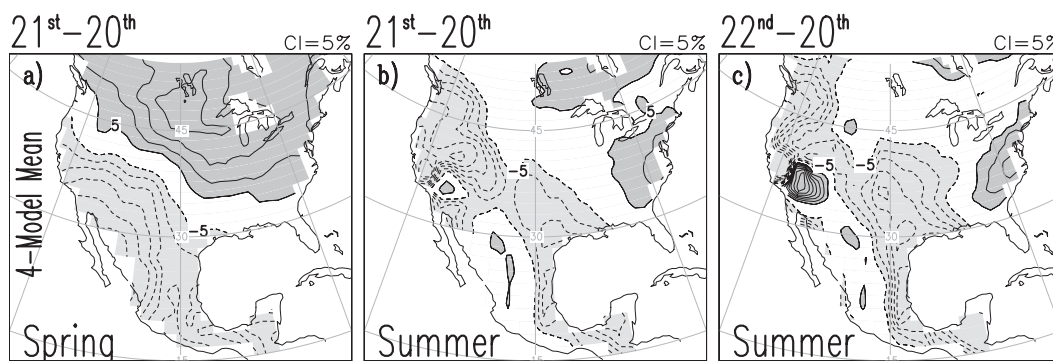


FIG. 3. Precipitation changes from four-model mean projections and simulations. Changes from models CCSM3, GFDL CM2.1, HadCM3, and ECHAM5/MPI-OM were used for the four-model mean regridded to a  $1.5^\circ \times 1.5^\circ$  grid. Changes are with respect to the twentieth-century seasons (1901–99). Changes in the (a) spring and (b) summer of the twenty-first century (2001–99), and the (c) summer of the twenty-second century (2101–99). Changes are given in percent units of the fractional changes, with a contour interval of 5%. Dark (light) shading denotes positive (negative) changes larger than  $|\pm 5|\%$ .

century. It is apparent that climatological spring precipitation in the twenty-first century, when compared with the spring of the twentieth century, will increase in parts of the United States, particularly in the eastern half and to the north of  $35^\circ\text{N}$ , and decrease over the U. S. southwest and Mexico. However, the structure of these differences is not coherent among the models. These results are consistent with those obtained by Cook et al. (2008), even though they used a different scenario. Differences in summer precipitation are less consistent. While CCSM3 and ECHAM5/MPI-OM suggest an increase in precipitation, largely over the central and southeastern portions of the United States, GFDL CM2.1 and HadCM3 indicate a decrease. Similarly, and except for ECHAM5/MPI-OM, a decrease along the Pacific Northwest coast of the United States and Canada is projected by the rest of the models. However, all of the models do agree on an increase in summer precipitation over the northeastern coast of the United States and a decrease along the eastern and southeastern portions of Mexico. Differences in the summer climatologies of the twenty-first century are exacerbated in the twenty-second century when carbon dioxide has been stabilized at its highest level.

The projected changes for the twenty-first-century agree with those of the multimodel mean from the latest assessment report by Solomon et al. (2007, chapter 11 and Fig. 11.12), even though the periods of comparison are different. Figure 3 displays the spring and summer percent changes (or fractional changes), with respect to the twentieth-century seasonal precipitation, from the mean of the four models analyzed here. The projected changes in spring of the twenty-first century are marked by a decrease in precipitation over all of Mexico and the U.S. Southwest, with a maximum over northwestern Mexico, as well as an increase in precipitation over the rest of the

United States and Canada. The projected changes in spring progress in a southwest–northeast direction in summer of the same century. A decrease in summer precipitation now covers the whole western, central, and southeastern regions of the United States and the Mexican coastal regions in the northwest, east, and south. Increased summer precipitation now occupies small pockets over the northeast/southeast) of the United States/Canada and central Mexico. Changes in summer precipitation for the twenty-second century are essentially similar to those in the twenty-first century, but larger. Agreement from a large percentage of the models from Solomon et al. (2007, chapter 11 and Fig. 11.2) exists over the following zones. Regions of decreased precipitation are found over the U.S. Pacific Northwest and southern and southeastern Mexico (17 or more out of 21 models), and a region of increased precipitation is found over the northeastern United States (14 or more out of 21 models); all models in the current study present the mentioned changes in precipitation. Agreement also exists over the central United States where the projected decrease in precipitation has a large uncertainty (between 8 and 13 out of 21 models; 2 out of 4 models in the present analysis). Thus, changes given by the 21-model mean used in Solomon et al. (2007) are very similar to changes given by a 4-model mean calculated with the models used here.

A couple of cautionary notes are needed here regarding the use of a figure like Fig. 3 and widely used in Solomon et al. (2007). The most obvious is that the multimodel mean may be the result of a set of only a few dominant models, so one has to be careful when drawing conclusions that represent the majority of the models. The less evident note is regarding the choice of how to represent the changes. The regions of maximum fractional changes displayed in Fig. 3 do not align with the

regions of maximum change seen in Fig. 2, and that may be misleading. For instance, the fractional changes in summer precipitation in Fig. 3 show a large decrease over California (middle panel), but the four maps in Fig. 2 (panels in middle column) show nothing close to this (i.e., conditions in the twenty-first century are very similar to those in the twentieth century with differences smaller than  $0.3 \text{ mm day}^{-1}$ ).

The large uncertainty in the projections of summer precipitation over the central United States is a reflection of the difficulty that the region imposes over the climate models. The difficulty arises from an unreal hierarchy of processes driving precipitation variability in some models (e.g., Ruiz-Barradas and Nigam 2006, 2010).

### c. Twentieth-century changes

One can only wonder whether the changes displayed by the projections of the climatological spring and summer precipitation have some resemblance with the observed changes in the twentieth century; similarities will give some reassurance of the projections. A second-order question, just for the time being, is whether the projected changes by the models are consistent with the changes simulated by them at the end of the twentieth century. The imposed changes in  $\text{CO}_2$  in the twentieth century are not as strong as those imposed in the twenty-first century under the A1B scenario, so the changes in spring and summer precipitation in the twentieth century are particularly sensitive to the ability of the coupled models to simulate natural variability of the global (and regional) climate. Thus, just because the natural variability in the models is still work in progress, it is fair to compare the projected changes in climatological spring and summer precipitation in the twenty-first century with respect to the observed changes (and not the simulated ones) of those seasons in the second half of the twentieth century. Changes in the century-long spring and summer climatologies of the twentieth century in observations and simulations have been calculated as the difference between the second-half (1951–99) minus the first-half (1901–50) of the century climatologies, as shown in Fig. 4. Observations show that spring precipitation, particularly over the Pacific Northwest, the central and eastern regions of the United States, and eastern Mexico, has been increasing, but in areas like the southwestern United States and southeastern Mexico spring precipitation has been decreasing in the second part of the century. In summers, however, the situation is reversed for some regions like the eastern and southeastern United States, where precipitation decreases, and for western, central, and southeastern Mexico, where summer precipitation increases in the second half of the twentieth century. On the other hand, the increase in spring precipitation in the

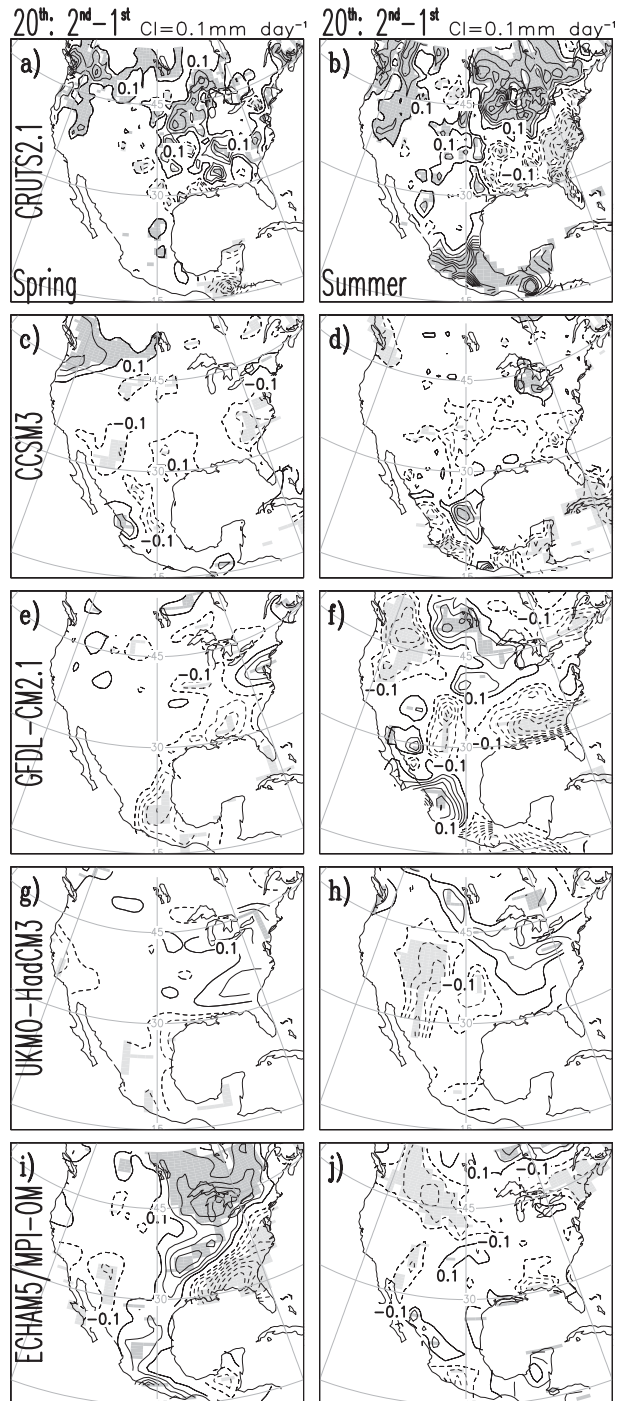


FIG. 4. Differences between the second (1951–99) and first (1901–50) halves in the twentieth century of climatological (left) spring and (right) summer precipitation from observations and coupled model simulations for (a),(b) CRUTS2.1, (c),(d) CCSM3, (e),(f) GFDL CM2.1, (g),(h) HadCM3, and (i),(j) ECHAM5/MPI-OM. Contour interval is  $0.1 \text{ mm day}^{-1}$ , and dark (light) shading denotes positive (negative) differences larger than  $|\pm 0.1| \text{ mm day}^{-1}$ . Note that the contour interval and the threshold of the shading are one-third those in Fig. 2. Shaded differences are significant according to a one-tailed Student's *t* test at the 0.10 level.

second half of the twentieth century is followed by an increase in summer precipitation over the Pacific Northwest and central regions of the United States, as well as in the eastern portion of Mexico.

The changes in spring and summer precipitation in the twentieth century simulated by the models are not consistent throughout and have limited resemblance with the observed changes. While CCSM3 and, to a lesser degree, ECHAM5/MPI-OM agree with observations on a wetter spring over the Pacific Northwest, HadCM3 and ECHAM5/MPI-OM, on the other hand, marginally reproduce the observed wetter eastern and central United States, respectively. The drying of southeastern Mexico in the spring is partially captured by both ECHAM5/MPI-OM and GFDL CM2.1. The observed wetter summer in the Pacific Northwest is only weakly captured by HadCM3. While the wetter north-central United States is captured in different ways by the models, the wetter central United States is partially captured by GFDL CM2.1 and ECHAM5/MPI-OM. Spring and summer changes in Mexico are not better represented by the models. While ECHAM5/MPI-OM weakly captures the observed wetter summer over the eastern and southern regions in Mexico, CCSM3 and GFDL CM2.1 only capture the wetter coasts to the east and west, respectively. The observed drying in the eastern United States in summer is weakly captured by CCSM3, while the drying over the southeastern United States is reasonably captured by GFDL CM2.1 and weakly by ECHAM5/MPI-OM.

Generally speaking, the significant changes in spring precipitation projected by the models for the twenty-first century, particularly a wetter north-central United States, a drier U. S. Southeast and a drier southeastern Mexico, resemble the similarly significant observed changes in spring precipitation in the second half of the twentieth century. The projected significant changes in summer for the twenty-first century have less correspondence with the significant observed changes in summer precipitation in the second half of the twentieth century than the corresponding changes in spring precipitation. Two models—CCSM3 and ECHAM5/MPI-OM—agree on a wetter north-central United States (Figs. 2b,k), while the other two models—GFDL CM2.1 and HadCM3—agree on a drier U.S. Southeast coast (Figs. 2e,h). The projected wetter U.S. Northeast in the summer of the twenty-first century is not backed up by the current observed drying tendency at the end of the twentieth century. A striking point is that the projected widespread drying of the western and southwestern United States in the summer of the twenty-first century, highlighted by the multimodel mean, has little support from the current tendency in precipitation observed in the second half of the twentieth century.

#### 4. Great Plains precipitation variability

The central United States is characterized by its large interannual variability in precipitation during the warm season (Ruiz-Barradas and Nigam 2005). Models, except for ECHAM5/MPI-OM, tend to displace this large center of variability to the west, as portrayed by the summer mean of monthly standard deviation of precipitation [not shown, but present in Ruiz-Barradas and Nigam (2006)].

Interannual variability of seasonal precipitation over the region can be captured and analyzed in two ways: first by calculating the regional standard deviation and second by developing a Great Plains precipitation index of seasonal anomalies from which a histogram of events can be obtained. The largest precipitation variability over the United States during the warm season can be located in the 35°–45°N, 100°–90°W box, and within the box the index can be created from area-averaged seasonal precipitation anomalies (Ruiz-Barradas and Nigam 2005, 2006). Similarly, spring and summer standard deviations can also be used to obtain area-averaged standard deviations using the same domain as for the Great Plains precipitation index from observations, simulations of the twentieth-century climate, and from projections of the twenty-first- and twenty-second-century climates, as shown in Tables 2 and 3. Variability in observations during spring is  $\sim 0.6 \text{ mm day}^{-1}$ , but model simulations of the twentieth-century climate provide a range of similar values, including  $0.5 \text{ mm day}^{-1}$  for CCSM3 and GFDL CM2.1,  $0.6 \text{ mm day}^{-1}$  for HadCM3, and  $0.8 \text{ mm day}^{-1}$  for ECHAM5/MPI-OM. On the other hand, summer variability is similar in the observations, HadCM3 and CCM3 ( $\sim 0.6 \text{ mm day}^{-1}$ ), but it is higher in GFDL CM2.1 ( $\sim 0.8 \text{ mm day}^{-1}$ ) and ECHAM5/MPI-OM ( $\sim 0.7 \text{ mm day}^{-1}$ ). Summer precipitation variability is practically the same as spring variability in the observations and HadCM3, but it is lower in ECHAM5/MPI-OM and it is higher in CCSM3 and GFDL CM2.1. It is interesting to point out that the largest variability in spring is seen in the ECHAM5/MPI-OM model, but the largest variability in summer is in the GFDL CM2.1 model; in both cases, the increase is above 40% with respect to the observed values, suggesting the presence of extreme events in the simulations by those models.

Precipitation variability over the Great Plains in the climate projections of the twenty-first and twenty-second centuries is more consistent throughout the models in spring than in summer when compared to twentieth-century variability. All of the models suggest that spring precipitation variability will increase in the twenty-first century but, excluding CCSM3, the rest of the models also indicate an increase in variability in the

TABLE 2. Spring standard deviation of precipitation over the Great Plains in observations and climate simulations of the twentieth century, and climate projections of the twenty-first and twenty-second centuries. Units are in  $\text{mm day}^{-1}$ .

Model	Twentieth century	Twenty-first century	Twenty-second century
CRUTS2.1	0.57	—	—
CCSM3	0.46	0.54	0.54
GFDL CM2.1	0.49	0.63	0.74
HadCM3	0.63	0.80	0.90
ECHAM5/MPI-OM	0.81	0.82	0.94

twenty-second century. There is less agreement among all of the models regarding summer precipitation variability in the twenty-first century. While GFDL CM2.1 and ECHAM5/MPI-OM suggest that summer precipitation variability in the twenty-first century remains the same as in the twentieth century, CCSM3 and HadCM3 both indicate an increase. Summer precipitation variability in the twenty-second century has conflicting results: while CCSM3 and ECHAM5/MPI-OM suggest an increase, GFDL CM2.1 and HadCM3 indicate a decrease. The increase in spring variability in the twenty-first century (Table 2) goes together with an increase in the spring precipitation, as can be seen by the positive changes (north of  $35^{\circ}\text{N}$  and east of  $100^{\circ}\text{W}$ ) in Figs. 2a,d,g,j. However, changes in summer variability are not directly associated with changes in the mean summer precipitation.

Inconsistencies in summer precipitation variability are related to a different hierarchy of processes generating that variability in the models. Spring and summer climatic conditions differ in the central United States by the intensity of the land surface–atmosphere feedback. In summer this feedback is stronger than in spring owing to the larger energy and moisture supplies over the region in summer (Nigam and Ruiz-Barradas 2006). Models tend to prioritize this mechanism as a generator of precipitation variability in summer via local evapotranspiration, which is not supported by observations (Ruiz-Barradas and Nigam 2005, 2006). Observations suggest a more important role of remote SSTs driving moisture fluxes as generators of summer precipitation variability by moisture flux convergence over the central United States. These model deficiencies result in the lack of coherence in summer precipitation variability as it was shown in a previous study (Ruiz-Barradas and Nigam 2006).

#### a. Extremes

The distribution of hydroclimate events, including extremes, is an important aspect of regional precipitation variability that deserves some attention. The presence

TABLE 3. Summer standard deviation of precipitation over the Great Plains in observations and climate simulations of the twentieth century, and climate projections of the twenty-first and twenty-second centuries. Units are in  $\text{mm day}^{-1}$ .

Model	Twentieth century	Twenty-first century	Twenty-second century
CRUTS2.1	0.60	—	—
CCSM3	0.64	0.76	0.84
GFDL CM2.1	0.82	0.82	0.63
HadCM3	0.61	0.68	0.60
ECHAM5/MPI-OM	0.66	0.65	0.87

of extreme events contributes toward a large regional standard deviation. Histograms of seasonal events that the Great Plains experiences and that the models simulate and project during spring and summer are displayed in Fig. 5. Spring and summer histograms of observations of the twentieth century, displayed as continuous thick black lines in all panels, highlight the large concentration of those seasons in the range from  $-1$  to  $+1 \text{ mm day}^{-1}$  for 91 out of 99 years in both cases.<sup>1</sup> Less apparent is the fact that there are more pluvial (53) than dry springs (46) and more dry (53) than pluvial (46) summers.

Spring and summer histograms from the twentieth-century simulations, displayed as dashed, thick black lines, show that HadCM3 has distributions similar to those observed, with 87 (90) springs (summers) out of 99 years in the  $-1$  to  $+1 \text{ mm day}^{-1}$  range. This model also produces a number of pluvial (dry) seasons: 51 (48) for spring and 48 (51) for summer, which are comparable to those in the observations. The spring histograms in the twentieth century from GFDL CM2.1 and ECHAM5/MPI-OM reveal contrasting distributions. While the former is narrow in the  $-1$  to  $+1 \text{ mm day}^{-1}$  range with 94 out of 99 events, the latter is wide in the same range of anomalies with 80 out of 99 events; this is also consistent with the spring standard deviation, which is small in GFDL CM2.1 and large in ECHAM5/MPI-OM. The distribution in the spring histogram from CCSM3 has the largest number of seasons (97 out of 99) in the  $-1$  to  $+1 \text{ mm day}^{-1}$  range owing to the large number of dry springs. Summer histograms in the twentieth-century simulations underestimate the number of seasons in the  $-1$  to  $+1 \text{ mm day}^{-1}$  range; GFDL CM2.1 has the lowest number of summers within this range (75 out of 99),

<sup>1</sup> Although the  $-1$  to  $+1 \text{ mm day}^{-1}$  range is arbitrary, it covers the range of spring and summer standard deviations shown in Tables 2 and 3. Thus, the difference between the total number of seasons (99) and the number of seasons tallied in the  $-1$  to  $+1 \text{ mm day}^{-1}$  range gives the number of seasons under extreme pluvial/dry conditions.

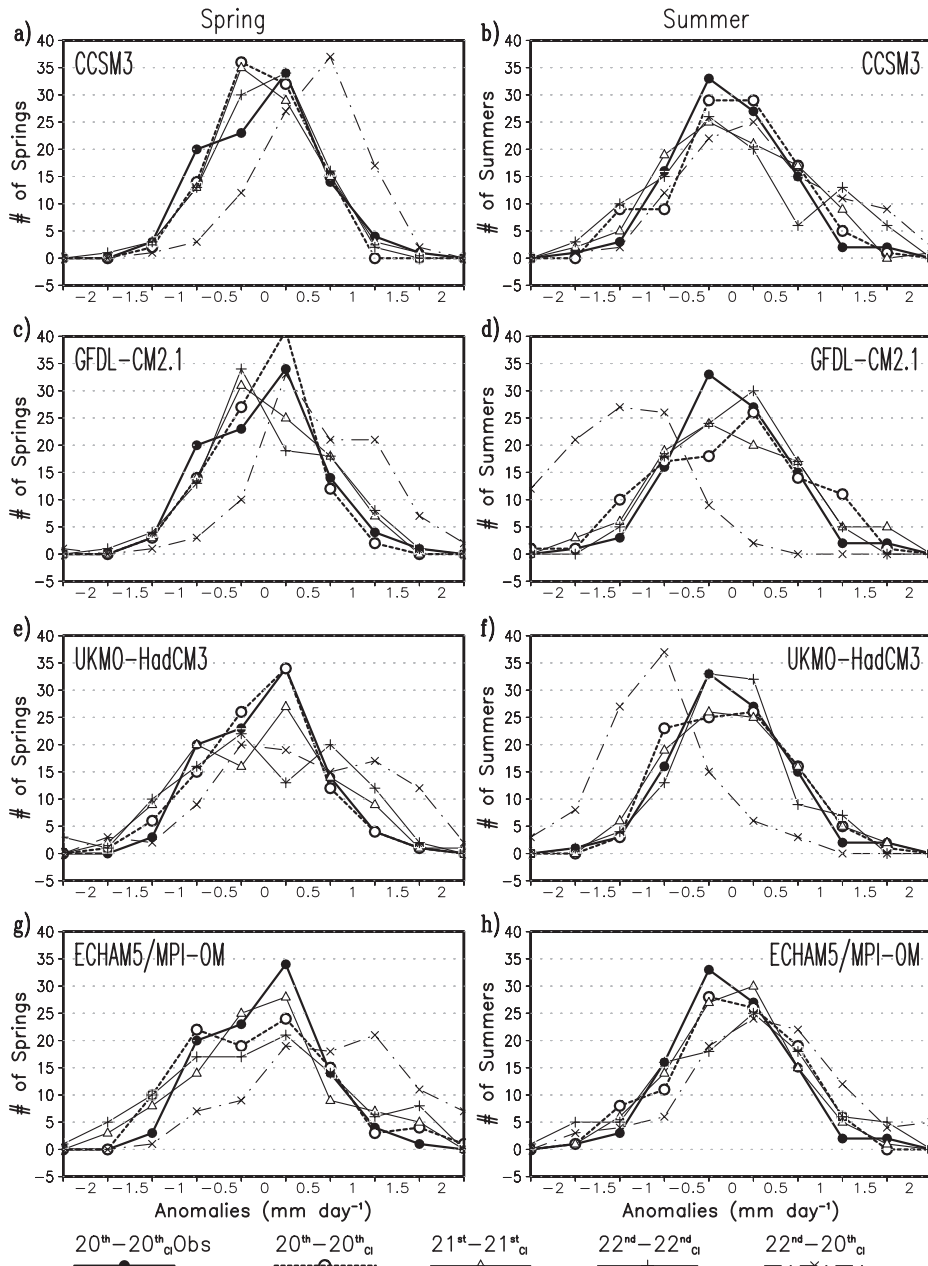


FIG. 5. Histogram of precipitation events over the Great Plains ( $35^{\circ}$ – $45^{\circ}$ N,  $100^{\circ}$ – $90^{\circ}$ W) as portrayed by the seasonal Great Plain precipitation index in observations and coupled model simulations of the twentieth century (1901–99), and projections of the twenty-first (2001–99) and twenty-second (2101–99) centuries in (left) spring and (right) summer. (a),(b) CCSM3, (c),(d) GFDL CM2.1, (e),(f) HadCM3, and (g),(h) ECHAM5/MPI-OM. Histograms of the simulations of the twentieth-century anomalies (thick, short-dashed line with open circles), projections of the twenty-first-century anomalies (thin continuous line with open triangles), and projections of the twenty-second-century anomalies (thin continuous line with plus signs) are plotted; seasonal anomalies used to create the indices of these histograms are with respect to climatologies of their corresponding century. For comparison purposes, the histogram from the observed CRUTS2.1 index has been plotted as a thick continuous line with filled circles, and the projections of the twenty-second-century seasonal anomalies, calculated with respect to the corresponding simulated twentieth-century seasonal climatologies, are plotted as a thin dash-dot line with multiplication signs. The x axis represents the anomalous events by categories of  $0.5 \text{ mm day}^{-1}$  and the y axis shows the number of seasons (springs or summers) that a given category of anomalies occurs.

consistent with the large summer standard deviation by the model.

The distribution of pluvial and dry seasons in the projected climates of the twenty-first and twenty-second centuries, as seen in the histograms, are not consistent throughout the models. However, changes in the spring histograms under the projected twenty-first-century climate, displayed as a continuous thin line with triangles, are consistent among the models when compared with histograms of their simulated twentieth-century climate. All of them suggest a decrease in the number of springs in the  $-1$  to  $+1$  mm day<sup>-1</sup> range and an increase in the  $+1$  to  $+2$  mm day<sup>-1</sup> range. The subsequent changes in spring histograms from the projected twenty-second-century climate, displayed as a continuous thin line with plus signs, suggest an additional decrease in the number of springs in the  $-1$  to  $+1$  mm day<sup>-1</sup> range and an increase in the  $+1$  to  $+2$  mm day<sup>-1</sup> range by the models, except by the slight decrease in the  $+1$  to  $+2$  mm day<sup>-1</sup> range shown by CCSM3. Changes in the number of summers in the  $-1$  to  $+1$  mm day<sup>-1</sup> range are less consistent throughout the models. While both CCSM3 and HadCM3 indicate a decrease in the number of such summers in the twenty-first century, GFDL CM2.1 and ECHAM5/MPI-OM suggest an increase. On the other hand, CCSM3 and ECHAM5/MPI-OM both suggest a decrease in the number of such summers in the twenty-second century, whereas GFDL CM2.1 and HadCM3 indicate an increase.

A clearer picture regarding the presence of extremes emerges when anomalies are calculated using the twentieth-century climatology. Changes from century to century are not included in the Great Plains precipitation anomalies that made the indices used to elaborate the histograms. The histograms for the projected distribution of springs and summers in the twenty-first and twenty-second centuries were obtained from the Great Plains precipitation anomalies calculated with respect to their own twenty-first- and twenty-second-century climatologies, as shown by the continuous thin lines with triangles and plus signs. The changes from century to century are incorporated in the Great Plains indices by calculating anomalies with respect to the model twentieth-century climatologies. In this case, the distributions in the twenty-second century, displayed as continuous thin lines with multiplication signs, show clear biases. There is a tendency toward wetter springs in all models and drier summers in GFDL CM2.1 and HadCM3, but wetter summers in CCSM3 and ECHAM5/MPI-OM. Histograms of the twenty-first century (not shown) display similar tendencies to those in the twenty-second-century histograms, but less shifted.

Thus, models tend to show that an increase in the number of extreme events, with respect to their twentieth-century climatology, impacts the changes in

the mean seasonal precipitation. However, consistency among the models is only seen for spring and not for summer projections. It is clear that the increased number of extreme pluvial springs in the  $+1$  to  $+2$  mm day<sup>-1</sup> range for the twenty-first and twenty-second centuries have a larger impact than the reduction of springs in the  $-1$  to  $+1$  mm day<sup>-1</sup> range for the projected increase in the mean spring precipitation over the central Great Plains (e.g., Fig. 2).

#### *b. Low-frequency precipitation variability*

Precipitation variability can drive droughty and pluvial conditions that can be exacerbated by the land surface conditions. A frequently used way to incorporate both of these factors in a single variable is by using the Palmer Drought Severity Index; however, it is not available from climate model simulations and projections.<sup>2</sup> Therefore, a proxy that mimics the PDSI is devised by means of maximizing the correlation between the PDSI and the proxy. By successive applications of a binomial filter to Great Plains indices of seasonal precipitation and PDSI anomalies, the proxy is obtained as a smoothed precipitation index.

Observed Great Plains indices of smoothed seasonal precipitation and PDSI anomalies that highlight interannual and longer time scales are displayed in Fig. 6. Both indices were smoothed by applying a 1–2–1 binomial filter 12 consecutive times.<sup>3</sup> Simultaneous correlation is 0.84, but precipitation leads PDSI by two seasons, in which case the correlation increases by 0.92. Thus, given the high correlation between the smoothed seasonal precipitation and PDSI indices over the Great Plains, the smoothed precipitation index can be used as a proxy for the seasonal PDSI index or, in other words, for the precipitation and land surface conditions. If the seasonal indices are not smoothed, then their correlation is 0.54, thus the importance of smoothing in creating the proxy. In view of these results, variability of the surface conditions from the climate simulations and projections can be generated via their corresponding smoothed seasonal precipitation indices (not shown).

Devastating hydroclimate events over the Great Plains include multiyear droughts, such as the spring–summer

<sup>2</sup> If potential evapotranspiration is properly calculated, that is, if it is not overestimated because the foretold increase in air temperature for the twenty-first-century climate projection, then the PDSI is still a valid tool to track meteorological droughts in the climate of the twenty-first century (Burke et al. 2006).

<sup>3</sup> If the filter is applied 50–55 times, then one can eliminate interannual variability of the indices and maximize decadal to interdecadal variability as well as the simultaneous correlation to 0.92. Precipitation leads PDSI by two seasons in which case the correlation slightly increases to 0.94.

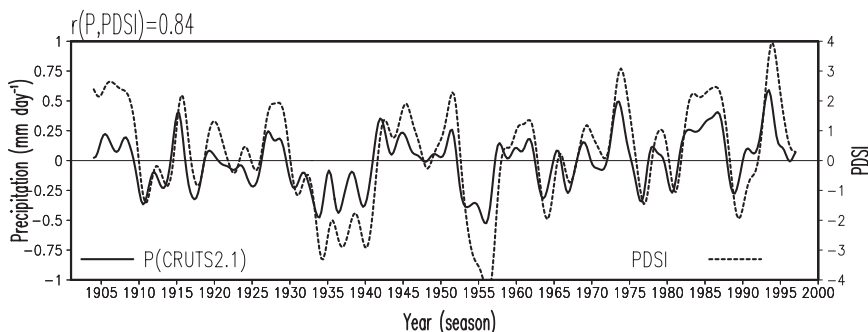


FIG. 6. Smoothed seasonal Great Plains precipitation and PDSI indices ( $35^{\circ}$ – $45^{\circ}$ N,  $100^{\circ}$ – $90^{\circ}$ W) during the twentieth century (1901–99). Precipitation index is from CRUTS2.1 and PDSI from the Dai dataset. The seasonal indices have been smoothed using a 1–2–1 binomial filter applied 12 times and have a correlation of 0.84 after smoothing. The simultaneous correlation between the seasonal indices increases from 0.54 without filtering to 0.92 when applying the filter 50 times. Precipitation leads PDSI by two seasons.

Dust Bowl in the 1930s and summer–fall season in the 1950s, and single-year pluvial events, such as those in 1993 and 2008, which, excluding the 2008 event, can be identified in Fig. 6. Simulation of such events is of great importance; however, doing so is a challenging task for global models. Using smoothed Great Plains precipitation indices from the climate simulations and projections, similar to the one from observations displayed in Fig. 6, it is possible to assess the total number of events that exceed one standard deviation during the spring–summer–fall period of every year<sup>4</sup> (Fig. 7). This portion of the year is chosen not only because more precipitation falls in the region, but also because the interannual variability of seasonal precipitation is maximum too; histograms using the whole year (not shown, i.e., including winter) have mostly minor changes in the twenty-second century. However, it should be pointed out that a preconditioning outside of the region and during the antecedent winter–spring portion of the year has been also important in some of those events.

Histograms of events, displayed in Fig. 7, indicate that all of the four models tend to underestimate the total number of extreme droughty events and to overestimate the total number of extreme pluvial events in the twentieth century; however, projections of the twenty-first and twenty-second centuries are varied among the models. Models like CCSM3 and ECHAM5/MPI-OM indicate an increase in droughty events in the twenty-first century, followed by a decrease in the twenty-second century; the number of droughty events in GFDL CM2.1 remains the same in the twenty-first century but, as in the other two

models, they also decrease in the twenty-second century. In HadCM3 a decrease in the number of droughty events in the twenty-first century and then an increase in the twenty-second century is projected. In the case of pluvial events, models like GFDL CM2.1 and HadCM3 project an equal number of events in the twentieth and twenty-first centuries that decrease in the twenty-second century; meanwhile, the number of pluvial events in CCSM3 decreases in the twenty-first century and decreases more in the twenty-second century. The number of pluvial events in ECHAM5/MPI-OM, GFDL CM2.1, and HadCM3 remains the same in the twentieth and twenty-first centuries, but increases in the twenty-second century.

## 5. Change and variability of SSTs

Change and variability of the regional precipitation is analyzed in terms of their contemporaneous SST structures.

### a. Change

The observed changes in climatological precipitation in the twentieth century (Fig. 3) are not the only changes in the climate system. Concurrent changes in other climatic variables, such as SSTs, are also evident. Figure 8 (left panels) shows changes in climatological summer SSTs from the first to the second half of the twentieth century in both observations and model simulations. The analysis of observed SSTs indicates that the differences between the second and the first half of the twentieth century have the signature of a linear warming trend [or a nonlinear trend, as shown in Fig. 13 of Guan and Nigam (2008)] with the following features: 1) maximum warming along the midlatitude ( $20^{\circ}$ – $50^{\circ}$ N) coastal regions in both Pacific and Atlantic Oceans with the largest over the

<sup>4</sup> The total number of events is made of single year events and multiyear events where anomalies exceed one standard deviation for at least two consecutive years.

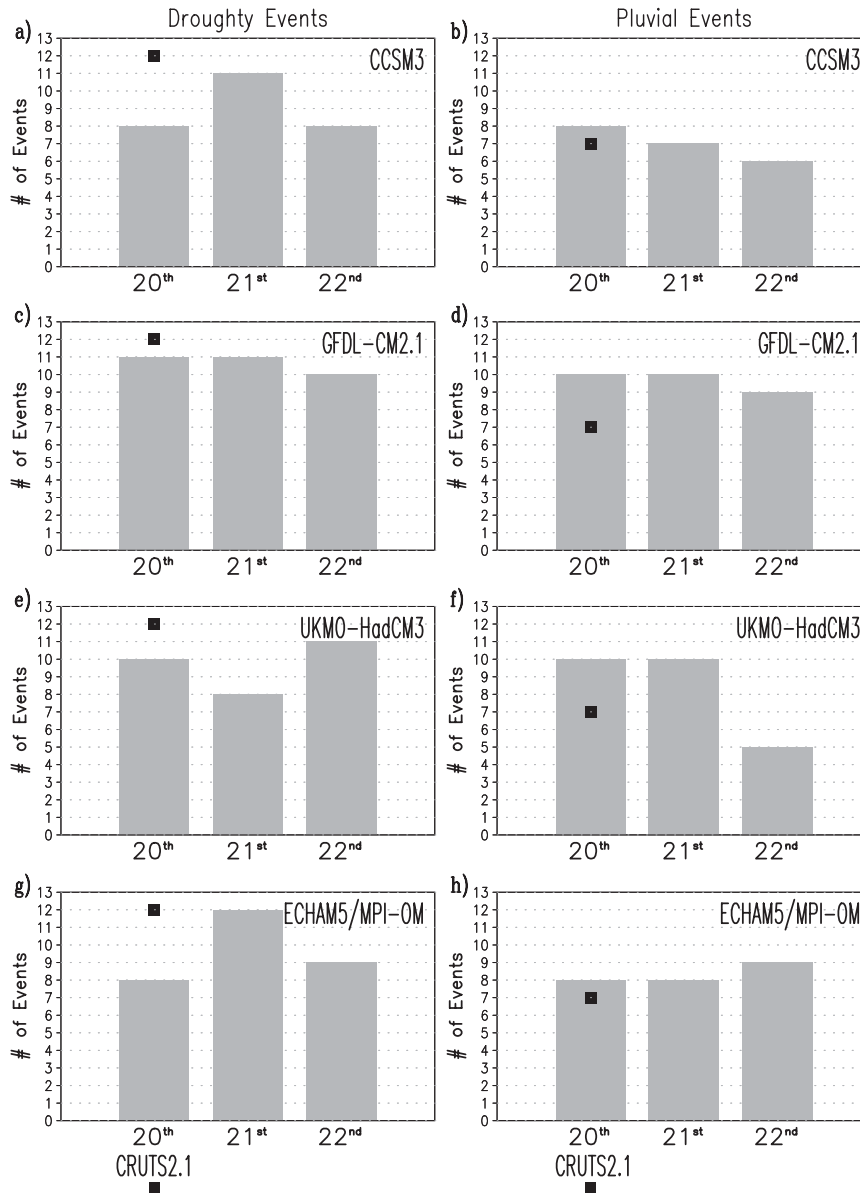


FIG. 7. Histograms of total (left) droughty and (right) pluvial spring–summer–fall events over the Great Plains ( $35^{\circ}$ – $45^{\circ}$ N,  $100^{\circ}$ – $90^{\circ}$ W) in observations and simulations of the twentieth-century climate, and projections of the twenty-first and twenty-second century climates. Events are tallied from smoothed precipitation indices (1–2–1 binomial filter applied 12 times) when the mean spring–summer–fall anomaly exceeds one standard deviation of the smoothed index in absolute value. The total number of events comprises multiyear events (when the exceeding anomaly stays for at least two consecutive years) and single-year events. Histograms from the models are organized as (a),(b) CCSM3, (c),(d) GFDL CM2.1, (e),(f) the HadCM3, and (g),(h) ECHAM5/MPI-OM. The histogram from the observed precipitation dataset CRUTS2.1 is marked (black square) in each panel, and the corresponding simulations and projections from the models are given (gray bars) above their corresponding labels marking the century.

Pacific, 2) maximum tropical coastal warming in the Indian and Atlantic Oceans, and 3) minimum tropical warming in the Pacific Ocean. Models, as was the case for the changes in precipitation, fail to reproduce those regions of maximum and minimum warming. While CCSM3 favors

high-latitude (north of  $40^{\circ}$ N) warming over both Pacific and Atlantic basins and warming in the tropical Pacific, GFDL CM2.1 favors maximum warming over the global tropical oceans and cooling over central midlatitudes in the Pacific Ocean. Warming in HadCM3 is larger in the

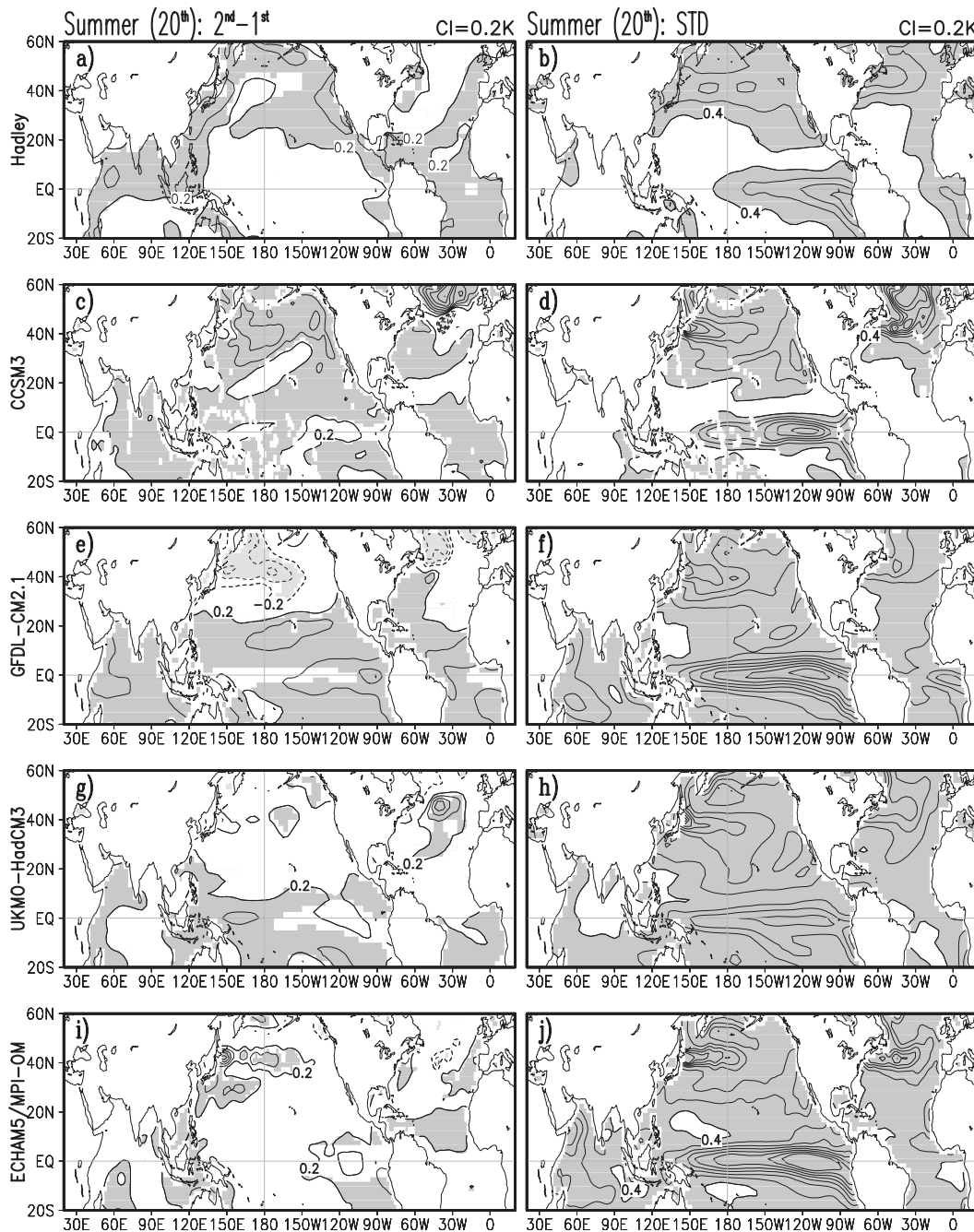


FIG. 8. Differences between the second (1951–99) and first (1901–50) halves of the twentieth century of the (left) climatological summer SSTs and (right) standard deviation of summer SSTs in the twentieth century (1901–99) from observations and coupled model simulations for (a),(b) Hadley Centre observations, (c),(d) CCSM3, (e),(f) GFDL CM2.1, (g),(h) HadCM3, and (i),(j) ECHAM5/MPI-OM. Contour interval is 0.2 K; dark (light) shading denotes positive (negative) differences larger than  $|\pm 0.2|$  K. Shaded differences are significant according a one-tailed Student's  $t$  test at the 0.10 level.

Atlantic midlatitudes than in the Pacific and warming in the tropical Pacific is larger than over the other tropical oceans. Warming in ECHAM5/MPI-OM in the Pacific Ocean is spread from the coastal midlatitudes to the

central and eastern Pacific; warming in the tropical Pacific is larger than in the Atlantic and Indian Oceans, with the tropical Atlantic warming appearing in the central basin. Thus, if the observed changes in climatological summer

precipitation are driven by the corresponding changes in SSTs, and are a consequence of the increase in greenhouse gases in the twentieth century, then the failure of the models to properly simulate the changes in SSTs are at the center of the poor simulation of the changes in summer precipitation.

### *b. Variability*

Before attempting to link precipitation variability over the Great Plains with SSTs of the neighboring oceans, a basic examination of the SST variability provides a quick assessment of the capabilities of the models. For that purpose the standard deviation of summer SSTs in the twentieth century is displayed in Fig. 8 (right panels) for both observations and model simulations. Interannual variability of summer SSTs in observations is the largest in the cold tongue region of the eastern equatorial Pacific ( $\sim 1$  K), followed by the midlatitudes of both the western Atlantic ( $\sim 0.8$  K) and central Pacific ( $\sim 0.8$  K), and, last, the eastern equatorial Atlantic ( $\sim 0.6$  K). While the maximum over the equatorial Pacific is associated with ENSO, those in the midlatitudes are ultimately associated with variability of the atmosphere [e.g., due to the Pacific–North America (PNA) or North Atlantic Oscillation (NAO)]. It is interesting to point out that the regions of maximum variability do not coincide with the regions of maximum warming trend (i.e., change in SST seen in the upper-left panel in Fig. 8), except for the coastal region of the western midlatitude Atlantic and, to a lesser degree, in the eastern Atlantic. Models tend to overemphasize and misplace variability over the equatorial Pacific as a consequence of the problems they have in simulating the ENSO evolution and structure (e.g., van Oldenborgh et al. 2005; Joseph and Nigam 2006). Variability over the midlatitude oceans is also overestimated and displaced; it is farther to the west and to the north of the position in observations. As a consequence, the simulated regional and global climates are affected (e.g., Barsugli et al. 2006).

## **6. SST links of Great Plains precipitation**

The structure of SST anomalies related to low-frequency precipitation variability over the Great Plains in the warm season is obtained by simultaneous correlation of summer global SST anomalies and smoothed summer Great Plains precipitation indices in observations and simulations of the twentieth-century climate (Fig. 9). The summer-only precipitation index is extracted from the smoothed seasonal precipitation index derived from the 1–2–1 binomial filter applied 12 times. Significant SST correlations from observations show a coherent basin-scale structure over the Pacific basin with both

tropical and extratropical imprints, similar to the Pacific decadal variability pattern; equally important are correlations over the subtropical and extratropical Atlantic basin. The features in both basins, with maximum correlations of 0.3, have been shown to play important roles in generating hydroclimate variability over the central United States (e.g., Barlow et al. 2001; Ruiz-Barradas and Nigam 2005; Wang et al. 2006; Schubert et al. 2009). Interestingly, the Great Plains also exhibits some connectivity with the Indian Ocean, which may be a reflection of the role that the tropics play in North Pacific interdecadal climate variability (e.g., Deser et al. 2004). The structure and sign of SST correlations with spring precipitation over the Great Plains (not shown) are very similar to those displayed in summer.

In general, all models reasonably capture the negative SST correlation structures over the extratropical Pacific and Atlantic Oceans, but the structure of the positive correlations, mainly in the Pacific basin, is more challenging. The broad structure of the positive correlations from the central Pacific to the western coast of Mexico seen in observations is absent in CCSM3. The absence of the positive correlations in CCSM3 is also mixed with negative correlations. Similarly, GFDL CM2.1 and HadCM3 display a region of negative correlations off the western coast of Mexico. The correlation structure seen in observations over the Pacific Ocean is best captured by ECHAM5/MPI-OM. On the other hand, the structure of positive correlations over the Caribbean Sea, the Indian Ocean, and the northern tropical Atlantic Ocean are reasonably captured by the models, although with a larger magnitude. The structure and sign of SST correlations with spring precipitation in the model simulations (not shown) do not differ by much from those in summer.

Before continuing with the analysis of the projections of the twenty-first and twenty-second centuries, it is necessary to pause here to emphasize that in the observations the regions of maximum summer SST variability in the twentieth century (Fig. 8, right panels) are not coincident with the regions of maximum correlation between SSTs and the Great Plains summer precipitation (Fig. 9). This is not surprising because the correlation structure in observations, with minimum correlations in the equatorial Pacific, rules out a contemporaneous link between summer Great Plains precipitation variability and ENSO, the latter highlighted in the standard deviation maps. In spite of the discrepancies between observations and models, the correlation structure in models also show the absence of an ENSO link of the Great Plains precipitation variability.

The correlation structure of seasonal SST anomalies associated with the low-frequency summer precipitation variability over the Great Plains seen in the simulations

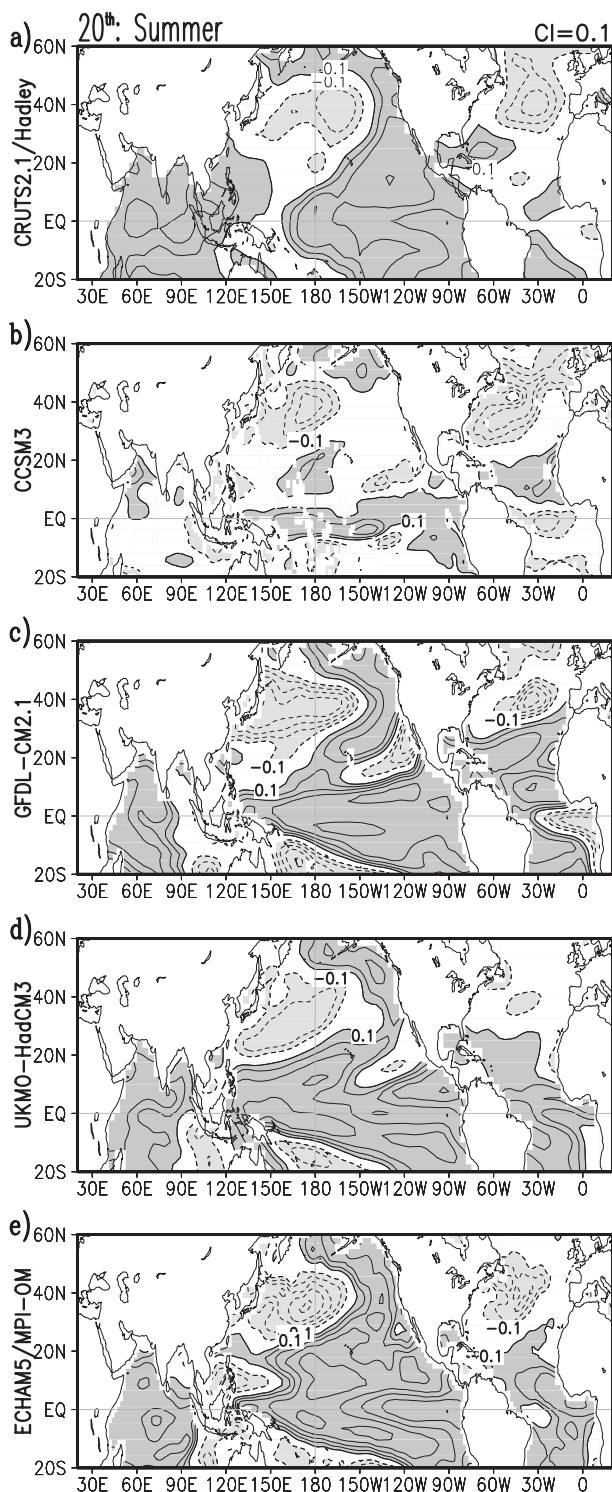


FIG. 9. Simultaneous summer SST correlations of the smoothed Great Plains precipitation index in observations and coupled model simulations during the twentieth century (1901–99). Unsmoothed summer SST anomalies are correlated with summer Great Plains indices ( $35^{\circ}$ – $45^{\circ}$ N,  $100^{\circ}$ – $90^{\circ}$ W) extracted after the all-season precipitation indices have been smoothed 12 times via a 1–2–1 filter: (a) Observed Hadley Centre SSTs and CRUTS2.1

of the twentieth-century climate is altered in the projections of the twenty-first- and twenty-second-century climates as shown in Fig. 10. The contrasting negative/positive SST correlation structures in both Pacific and Atlantic Oceans are practically nonexistent under the rapid increase of  $\text{CO}_2$  during the twenty-first century; that is, the cooling regions in the midlatitude and subtropical regions are being warmed. As revealed in the right panels, once the  $\text{CO}_2$  concentrations are stabilized in the twenty-second century, the contrasting negative/positive correlation structures tend to recover toward their conditions in the twentieth century. Similarly, the SST correlations with spring precipitation (not shown) display a decrease in magnitude in the twenty-first century and a recovery in the twenty-second century, mostly in the negative correlations in the midlatitude and subtropical regions.

The broad tropical warming stirs the global atmosphere in both the observations and model simulations. The surface tropical warming leads to enhanced 200-mb geopotential heights in the global tropics but reduced heights in the midlatitudes over both hemispheres, as displayed by the four-model mean in Fig. 11, and as shown in Schubert et al. (2004) and Seager et al. (2005). A ridge, straddling the south and east of the United States, is a feature in the simulations, except in CCSM3 that has the lowest tropical warming from the models analyzed. As in the case of the midlatitude negative SST correlations, the reduced heights at midlatitudes are raised during the warming of the twenty-first century and reduced back in the twenty-second century.

The same sign correlations (i.e., SST anomalies) over both tropical Pacific and Atlantic basins set up conditions for seasonal anomalous hydroclimatic events during the twenty-first- and twenty-second-century climates. As mentioned in the introduction, if both basins have the same sign, they are still capable of producing extreme hydroclimatic conditions over the central United States. This is partially seen in spring when there is an increase in extreme events in the twenty-first and twenty-second centuries, as illustrated by the histograms in Fig. 5. However, it must not be forgotten that precipitation variability, and so the occurrence of extremes, in the coupled model simulations and projections are not only

←  
precipitation index, (b) CCSM3, (c) GFDL CM2.1, (d) HadCM3, and (e) ECHAM5/MPI-OM. Contour interval is 0.1; dark (light) shading denotes positive (negative) correlations larger than  $|\pm 0.1|$ . A two-tailed Student's  $t$  test at the 0.05 (0.10) level indicates significant correlations equal or larger than 0.19 (0.17).

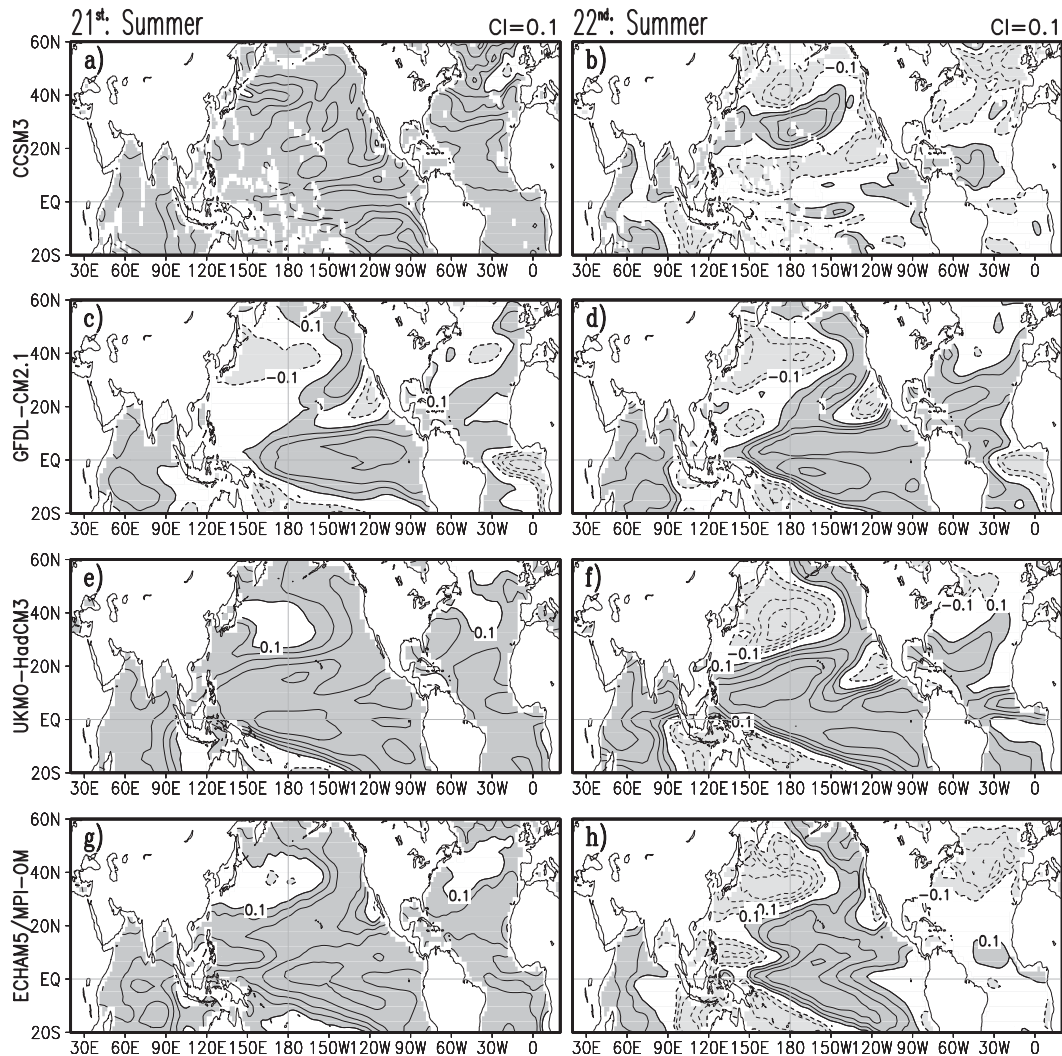


FIG. 10. Simultaneous summer SST correlations of the smoothed Great Plains precipitation index in projections of the (left) twenty-first (2001–99) and (right) twenty-second (2101–99) centuries. Unsmoothed summer SST anomalies are correlated with summer Great Plains indices extracted after the all-season precipitation indices have been smoothed 12 times via the 1–2–1 filter: (a),(b) CCSM3, (c),(d) GFDL CM2.1, (e),(f) HadCM3, and (g),(h) ECHAM5/MPI-OM. Contour interval is 0.1, and dark (light) shading denotes positive (negative) correlations larger than  $|\pm 0.1|$ . A two-tailed Student's  $t$  test at the 0.05 (0.10) level indicates significant correlations equal or larger than 0.19 (0.17). Anomalies in the indices and SSTs are with respect to the climatologies of the corresponding centuries.

dependent on the ocean but also on the modeled internal atmospheric variability and land surface–atmosphere variability as well.

The nature of the differences between the structures of the SST correlations with precipitation variability over the Great Plains is linked to the warming trend driven by the imposed increase in carbon dioxide. This is suggested from those correlations for the twenty-first-century climate but becomes apparent after detrending the data (not shown). After taking the linear trend out from both precipitation indices and SSTs, the correlation patterns that emerge in the twenty-first century lose the generalized

positive correlations and look more like those in the twentieth and twenty-second centuries. The change in magnitude of the correlations in the twenty-first century reaches the 0.1–0.2 range in absolute value, especially over the midlatitudes of the Pacific Ocean, except in the GFDL CM2.1 model<sup>5</sup> whose changes occur in the tropical latitudes of both the Pacific and Atlantic Oceans.

<sup>5</sup> In fact, the Great Plains precipitation index from GFDL CM2.1 is the only one among the precipitation indices from the four models analyzed here that has a negative trend in the twenty-first century.

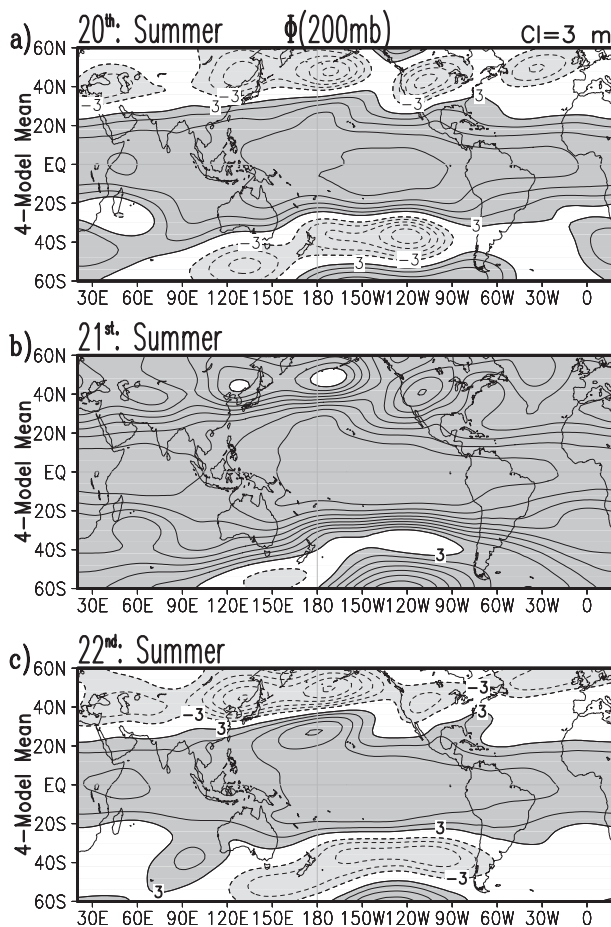


FIG. 11. Summer regressions of smoothed Great Plains precipitation indices on geopotential height anomalies at 200 mb from the four-model mean projections and simulations. Models CCSM3, GFDL CM2.1, HadCM3, and ECHAM5/MPI-OM were used for the four-model mean regridded to a common  $1.5^{\circ} \times 1.5^{\circ}$  grid: (a) twentieth century (1901–99), (b) twenty-first century (2001–99), and (c) twenty-second century (2101–99). Contour interval is 3 m, and dark (light) shading denotes positive (negative) anomalies larger than  $|\pm 3|$  m. All four models show similar structures to the four-model mean, with CCSM3 having the weakest tropical response among the models.

On the other hand, the structures of the SST correlations in the twentieth and twenty-second centuries do not change as much as in the twenty-first century in the models. However, the effect of extracting the trend for the twentieth century is much larger in the observations than in the model simulations. Changes in observations, after detrending the precipitation indices and SSTs, are in the 0.08–0.12 range in absolute value but in the 0.04–0.06 range in the models. More important is the fact that the warming seen in the deep tropical Atlantic in the twentieth century disappears in the observations but not in the simulations; similarly,

the warming displayed in the Indian Ocean is reduced but remains almost without change in the model simulations.

It is significant that coupled models can capture, albeit imperfectly, the links of summer precipitation over the Great Plains with SSTs over the Pacific and Atlantic Oceans. As mentioned in the introduction, such links have been established in observations and atmospheric models forced with observed or idealized SSTs. However, deficiencies in the coupled models to capture ENSO variability (e.g., Joseph and Nigam 2006; Merryfield 2006), Pacific Decadal variability (e.g., Furtado et al. 2011), and tropical Atlantic variability (e.g., Breugem et al. 2006) may be preventing them from better portraying those links. In addition, while the warm-season precipitation variability over the Great Plains in the models is related to SST anomalies over both Pacific and Atlantic basins, as observations indicate, overactive land surface–atmosphere interactions in those models may be preventing them from a better simulation of the observed precipitation variability (Ruiz-Barradas and Nigam 2005, 2006).

## 7. Concluding remarks

The present study has analyzed climatological spring and summer precipitation over North America, precipitation variability over the Great Plains and its summer SST links from observations, simulations of the twentieth-century climate, and projections of the twenty-first- and twenty-second-century climates under the A1B scenario. Under this scenario, carbon dioxide increases rapidly in the twenty-first century until it reaches almost twice its initial value at the end of the century to remain at this point during the twenty-second century.

- The dry west and humid east conditions observed in the United States in spring and summer cannot be accurately simulated by the models. Opposite of what is observed, models tend to produce wetter springs over the western United States and wetter summers over the central United States. However, all four of the models simulate the spring maximum over the U.S. Pacific Northwest and its subsequent disappearance in summer reasonably well. Models are also relatively successful in simulating the increase in precipitation over Mexico, especially over the western coast, from spring to summer; however, they fail to do so over the eastern coast.
- The projected changes in spring precipitation for the twenty-first century, including a wetter north-central United States, a drier southwestern United States, and a drier southeastern Mexico, agree in with the observed tendencies in spring precipitation in the second half of the twentieth century. However, the projected changes

in summer for the twenty-first century find little support from the observed tendencies in summer precipitation in the second half of the twentieth century. The projected changes in climatological precipitation are accompanied with changes in the occurrence of extreme seasonal events over the central Great Plains. That is, projected springs in the twenty-first and twenty-second centuries will be wetter as compared to those in the twentieth century, with an increase in wet springs in the 1–2 mm day<sup>-1</sup> range. Interestingly, this subset of four models portrays the results drawn from the complete set of 21 models used in Solomon et al. (2007) remarkably well.

- The observed changes in climatological precipitation are associated with characteristic SST structures seen as the footprint of global warming. The coastal regions of the midlatitude Pacific and Atlantic Oceans suffer the largest warming with no important changes along the equator. The change in summer SSTs in the twentieth-century climate simulations are deficient; the GFDL CM2.1 is the only one that has cooling rather than warming over the midlatitude oceans!
- Precipitation variability over the United States, as portrayed by seasonal standard deviation, experiences its largest values throughout the central region of the United States, that is, over the Great Plains (35°–45°N, 100°–90°W). Spring and summer standard deviations over this region in the twentieth century are captured with some difficulty by the models. While the HadCM3 has a distribution of seasonal events close to observations, ECHAM5/MPI-OM and GFDL CM2.1 have the largest spring and summer variability as a result of extreme seasonal events. On the other hand, all models project an increase in spring precipitation variability in the twenty-first century and, except for CCSM3, the models project an additional increase of spring variability for the twenty-second century. Projected summer precipitation variability lacks coherence among the models.
- Models have difficulties in simulating long-term droughts and pluvial events over the Great Plains. Simulations of the twentieth-century climate tend to underestimate the observed number of droughty events, and overestimate the number of pluvial events. Events from the projections of the twenty-first- and twenty-second-century climates do not show consistency among the four models.
- Climate models can portray, with varied degrees of success, the SST links of summer Great Plains precipitation seen in observations and atmospheric model simulations forced with historical SSTs. Pluvial events in observations are associated with SST features in the Pacific that resemble those from the Pacific decadal pattern with positive anomalies at tropical and subtropical latitudes close to the western coast of Mexico and the United States, and negative anomalies over the central midlatitudes. Atlantic SST features include positive SST anomalies over the tropics, including the Gulf of Mexico, and negative SST anomalies over the central midlatitudes. The SST features are reversed for droughty events. All models capture the observed SST structures in the central midlatitudes of the Pacific and Atlantic Oceans, but have some problems with the broad SST structure in the tropical and subtropical Pacific and the confined SST structure in the deep tropical Atlantic. The most successful model is ECHAM5/MPI-OM, while the least successful is CCSM3. Interestingly, the positive SST correlations in the deep tropical Atlantic are related to the linear trend in observations but not in the models.
- Here it is important to highlight that the SST correlation structures seen in both observations and simulations of the twentieth-century climate lack an equatorial ENSO footprint. This is in spite of the exaggerated variability along the equatorial Pacific in the simulations. Maximum SST variability in observations and simulations cover similar regions of the equatorial Pacific and Northern Hemisphere midlatitude oceans, but the magnitude in the simulations is much larger than in observations.
- The contrasting positive and negative SST structures in both Pacific and Atlantic Oceans, associated with summer precipitation variability over the Great Plains in the twentieth century, are almost removed in the projections of the twenty-first century and are recovered, to some extent, in the twenty-second century. This is due to the generalized increased warming in the twenty-first century and its subsequent stabilization in the twenty-second century. That is, the linear trend obscures the contrasting SST structures in both Pacific and Atlantic Oceans.
- The surface warming in the tropics associated with the summer precipitation variability over the central United States in simulations of the twentieth-century climate is associated with raised geopotential heights at 200 mb in the global tropics and decreased heights at the midlatitudes of both hemispheres. Among the models, CCSM3 has the weakest tropical response. The atmospheric response is similar to that identified in observations and atmospheric simulations forced with historical SSTs. The linear trend, as in the case of the SSTs, conceals the midlatitude decrease in heights in the twenty-first century and does little in the twentieth and twenty-second centuries.

In summary, one can see more consistent simulations and projections in spring than in summer over North

America, particularly over the central United States. Previous findings have shown that summer precipitation variability over the Great Plains imposes a challenge for state-of-the-art climate models because many of them prioritize local land surface–atmosphere interactions over remote SST–moisture flux convergence interactions at interannual-to-larger scales, which is at odds with observations. However, and in spite of those deficiencies and others involving global teleconnections, the climate models seem to possess the mechanisms that link summer precipitation variability over the central United States with the oceans. Thus, it must be a priority to have those interactions correct in climate models in order to improve simulations of summer precipitation variability over the central United States.

*Acknowledgments.* This research was funded by NSF, NOAA, NASA, and DOE as a Drought in Coupled Models Project (DRICOMP) grant (NSF ATM 0738907) under the U.S. CLIVAR Program (<http://www.usclivar.org>). The authors wish to acknowledge support from the DOE Grant DEFG0208ER64548. Likewise, we acknowledge to the modeling groups, the Program for Climate Model Diagnosis and Intercomparison (PCMDI), and the WCRP's Working Group on Coupled Modeling (WGCM) for their roles in making the WCRP CMIP3 multimodel dataset available. Support of this dataset is provided by the Office of Science, U.S. Department of Energy. Finally, the authors want to thank the anonymous reviewers for their constructive comments that helped to improve the quality of the paper.

#### REFERENCES

- Barlow, M., S. Nigam, and E. H. Berbery, 2001: ENSO, Pacific decadal variability, and U.S. summertime precipitation, drought, and streamflow. *J. Climate*, **14**, 2105–2128.
- Barsugli, J. J., S.-I. Shin, and P. D. Sardeshmukh, 2006: Sensitivity of global warming to the pattern of tropical ocean warming. *Climate Dyn.*, **27**, 483–492, doi:10.1007/s00382-006-0143-7.
- Breugem, W.-P., W. Hazeleger, and R. J. Haarsma, 2006: Multimodel study of tropical Atlantic variability and change. *Geophys. Res. Lett.*, **33**, L23706, doi:10.1029/2006GL027831.
- Burke, E. J., S. J. Brown, and N. Christidis, 2006: Modeling the recent evolution of global drought projections for the twenty-first century with the Hadley Centre climate model. *J. Hydrometeorol.*, **7**, 1113–1125.
- Collins, W. D., and Coauthors, 2006: The Community Climate System Model Version 3 (CCSM3). *J. Climate*, **19**, 2122–2143.
- Cook, K. H., E. K. Vizy, Z. S. Launer, and C. M. Patricola, 2008: Springtime intensification of the Great Plains low-level jet and Midwest precipitation in GCM simulations of the twenty-first century. *J. Climate*, **21**, 6321–6340.
- Dai, A., K. E. Trenberth, and T. Qian, 2004: A global dataset of Palmer Drought Severity Index for 1870–2002: Relationship with soil moisture and effects of surface warming. *J. Hydrometeorol.*, **5**, 1117–1130.
- Delworth, T. L., and Coauthors, 2006: GFDL's CM2 global coupled climate models. Part I: Formulation and simulation characteristics. *J. Climate*, **19**, 643–674.
- Deser, C., A. S. Phillips, and J. W. Hurrell, 2004: Pacific interdecadal climate variability: Linkages between the tropics and the North Pacific during boreal winter since 1900. *J. Climate*, **17**, 3109–3124.
- Enfield, D. B., A. M. Mestas-Núñez, and P. J. Trimble, 2001: The Atlantic multidecadal oscillation and its relation to rainfall and river flows in the continental U.S. *Geophys. Res. Lett.*, **28**, 2077–2080.
- Furtado, J. C., E. Di Lorenzo, N. Schneider, J. E. Overland, and N. A. Bond, 2011: North Pacific decadal variability and climate change in the IPCC AR4 models. *J. Climate*, in press.
- Gordon, C., C. Cooper, C. A. Senior, H. Banks, J. M. Gregory, T. C. Johns, J. F. B. Mitchell, and R. A. Wood, 2000: The simulation of SST, sea ice extents and ocean heat transports in a version of the Hadley Centre coupled model without flux adjustments. *Climate Dyn.*, **16**, 147–168.
- Guan, B., and S. Nigam, 2008: Pacific sea surface temperatures in the twentieth century: An evolution-centric analysis of variability and trend. *J. Climate*, **21**, 2790–2809.
- Hoerling, M., and A. Kumar, 2003: The perfect ocean for drought. *Science*, **299**, 691–694.
- Joseph, R., and S. Nigam, 2006: ENSO evolution and teleconnections in IPCC's twentieth-century climate simulations: Realistic representation? *J. Climate*, **19**, 4360–4377.
- Marsland, S., H. Haak, J. Jungclaus, M. Latif, and F. Röske, 2003: The Max-Planck-Institute global ocean/sea ice model with orthogonal curvilinear coordinates. *Ocean Modell.*, **5**, 91–127.
- McCabe, G. J., M. A. Palecki, and J. L. Betancourt, 2004: Pacific and Atlantic Ocean influences on multidecadal drought frequency in the United States. *Proc. Natl. Acad. Sci. USA*, **101**, 4136–4141.
- , J. L. Betancourt, S. T. Gray, M. A. Palecki, and H. G. Hidalgo, 2008: Associations of multi-decadal sea-surface temperature variability with US drought. *Quat. Int.*, **188**, 31–40.
- Meehl, G. A., C. Covey, T. Delworth, M. Latif, B. McAvaney, J. F. B. Mitchell, R. J. Stouffer, and K. E. Taylor, 2007: The WCRP CMIP3 multi-model dataset: A new era in climate change research. *Bull. Amer. Meteor. Soc.*, **88**, 1383–1394.
- Merryfield, W. J., 2006: Changes to ENSO under CO<sub>2</sub> doubling in a multimodel ensemble. *J. Climate*, **19**, 4009–4027.
- Mitchell, T. D., 2005: An improved method of constructing a database of monthly climate observations and associated high resolution grids. *Int. J. Climatol.*, **25**, 693–712.
- Nakicenovic, N., and Coauthors, 2000: *Special Report on Emissions Scenarios*. N. Nakicenovic and R. Swart, Eds., Cambridge University Press, 612 pp.
- Nigam, S., and A. Ruiz-Barradas, 2006: Seasonal hydroclimate variability over North America in global and regional reanalysis and AMIP simulations: Varied representation. *J. Climate*, **19**, 815–837.
- Pope, V. D., M. L. Gallani, P. R. Rowntree, and R. A. Stratton, 2000: The impact of new physical parameterizations in the Hadley Centre climate model—HadAM3. *Climate Dyn.*, **16**, 123–146.
- Rayner, N. A., D. E. Parker, E. B. Horton, C. K. Folland, L. V. Alexander, D. P. Rowell, E. C. Kent, and A. Kaplan, 2003: Global analyses of sea surface temperature, sea ice, and night marine air temperature since the late nineteenth century. *J. Geophys. Res.*, **108**, 4407, doi:10.1029/2002JD002670.

- Roeckner, E., and Coauthors, 2003: The atmospheric general circulation model ECHAM5. Part I: Model description. Max Planck Institute for Meteorology Rep. 349, 140 pp. [Available online at [http://www.mpimet.mpg.de/fileadmin/publikationen/Reports/max\\_scirep\\_349.pdf](http://www.mpimet.mpg.de/fileadmin/publikationen/Reports/max_scirep_349.pdf).]
- Ruiz-Barradas, A., and S. Nigam, 2005: Warm-season precipitation variability over the U.S. Great Plains in observations, NCEP and ERA-40 reanalyses, and NCAR and NASA atmospheric model simulations. *J. Climate*, **18**, 1808–1830.
- , and —, 2006: IPCC's twentieth-century climate simulations: Varied representations of North American hydroclimate variability. *J. Climate*, **19**, 4041–4058.
- , and —, 2010: SST–North American hydroclimate links in AMIP simulations of the Drought Working Group models: A proxy for the idealized drought modeling experiments. *J. Climate*, **23**, 2585–2598.
- Schubert, S. D., M. J. Suarez, P. J. Pegion, R. D. Koster, and J. T. Bacmeister, 2004: Causes of long-term drought in the U.S. Great Plains. *J. Climate*, **17**, 485–503.
- , and Coauthors, 2009: A U.S. CLIVAR project to assess and compare the responses of global climate models to drought-related SST forcing patterns: Overview and results. *J. Climate*, **22**, 5251–5272.
- Seager, R., Y. Kushnir, C. Herweijer, N. Naik, and J. Velez, 2005: Modeling of tropical forcing of persistent droughts and pluvials over western North America: 1856–2000. *J. Climate*, **18**, 4065–4088.
- Solomon, S., D. Qin, M. Manning, Z. Chen, M. Marquis, K. B. Averyt, M. Tignor, and H. L. Miller, Eds., 2007: *Climate Change 2007: The Physical Science Basis*. Cambridge University Press, 996 pp.
- Sutton, R. T., and D. L. R. Hodson, 2005: Atlantic Ocean forcing of North American and European summer climate. *Science*, **309**, 115–118.
- Ting, M., and H. Wang, 1997: Summertime U.S. precipitation variability and its relation to Pacific sea surface temperature. *J. Climate*, **10**, 1853–1873.
- van Oldenborgh, G. J., S. Y. Philip, and M. Collins, 2005: El Niño in a changing climate: A multi-model study. *Ocean Sci.*, **1**, 81–95.
- Wang, C., D. B. Enfield, S.-K. Lee, and C. W. Landsea, 2006: Influences of the Atlantic warm pool on Western Hemisphere summer rainfall and Atlantic hurricanes. *J. Climate*, **19**, 3011–3028.
- Weaver, S. J., and S. Nigam, 2008: Variability of the Great Plains low-level jet: Large-scale circulation context and hydroclimate impacts. *J. Climate*, **20**, 1532–1551.